PCCP

Cite this: *Phys. Chem. Chem. Phys.*, 2012, **14**, 6200–6210

www.rsc.org/pccp

PAPER

Ultrafast spectroscopy with sub-10 fs deep-ultraviolet pulses

Takayoshi Kobayashi*[abcd] and Yuichiro Kida†[ab]

Received 19th November 2011, Accepted 7th February 2012
DOI: 10.1039/c2cp23649d

Time-resolved transient absorption spectroscopy with sub-9 fs ultrashort laser pulses in the deep-ultraviolet (DUV) region is reported for the first time. Single 8.7 fs DUV pulses with a spectral range of 255–290 nm are generated by a chirped-pulse four-wave mixing technique for use as pump and probe pulses. Electronic excited state and vibrational dynamics are simultaneously observed for an aqueous solution of thymine over the full spectral range using a 128-channel lock-in detector. Vibrational modes of the electronic ground state and excited states can be observed as well as the decay dynamics of the electronic excited state. Information on the initial phase of the vibrational modes is extracted from the measured difference absorbance trace, which contains oscillatory structures arising from the vibrational modes of the molecule. Along with other techniques such as time-resolved infrared spectroscopy, spectroscopy with sub-9 fs DUV pulses is expected to contribute to a detailed understanding of the photochemical dynamics of biologically significant molecules that absorb in the DUV region such as DNA and amino acids.

1. Introduction

In the deep-ultraviolet (DUV) region from 200 nm to 300 nm, many basic aromatic molecules absorb radiation and undergo photochemical reaction. One of the most important examples in terms of human health is reaction of the biologically significant molecules DNA and RNA. These molecules absorb DUV light from the sun, leading to photodamage.[1,2] The photodamage process has been investigated extensively and a thymine dimer identified as one of the photoproducts.[3–5] At the same time, it is known that DNA has relatively high photostability, attributed to the ultrafast non-radiative relaxation dynamics of its building blocks, the nucleobases.[6] The time scale of this relaxation is in the sub-picosecond regime resulting also in a low fluorescence quantum yield. A variety of techniques, including transient absorption spectroscopy,[3,7–10] time-resolved fluorescence spectroscopy,[9,11,12] and time resolved infrared (IR) spectroscopy,[4,13–16] have been utilized to elucidate the photochemical dynamics of DNA and its nucleobases.

Despite the extensive investigations performed to date, the photochemical dynamics of these molecules have not been fully understood, and even the dynamics of a simple nucleobase such as cytosine remain unclear.[6] The time resolution of such spectroscopic techniques is limited by the pulse duration of the excitation and probe pulses, in particular by the duration of the DUV pump pulse (several tens of femtoseconds). Probing the ultrafast decay dynamics faster than 100 fs has been difficult.

In the visible spectral range, sub-10 fs visible pulses can be readily obtained and utilized in transient absorption spectroscopy. The vibrational dynamics and electronic excited state dynamics of various molecules have been probed with a time resolution of a few femtoseconds.[17–22] Phase information on the molecular vibrations, which cannot be obtained in time-resolved IR spectroscopy or Raman spectroscopy, can be acquired and used to assign each vibrational mode as an electronic excited state or a ground state. Extension of sub-10 fs spectroscopy to the DUV region would help elucidate the photochemical dynamics of biologically relevant molecules by giving complementary information to that obtained with time-resolved IR spectroscopy. A time resolution of better than 10 fs would also enable resolution of ultrafast electronic excited state dynamics, which occur much faster than 100 fs and would even provide information on real-time vibrational dynamics.

Spectroscopy with sub-10 fs DUV pulses, however, has not been reported to date although approaches for generating the pulses have been reported from several groups.[23–28] A fundamental difficulty has been in the removal of group-velocity dispersion, including high-order dispersion in the DUV wavelength region, which is much larger than in the visible region. The sub-10 fs pulse is readily broadened and distorted before it reaches the sample position in pump–probe spectroscopy. To obtain sub-10 fs DUV pulses at the sample, an approach based on the broadband chirped-pulse four-wave mixing (FWM) method has been proposed. By this method a single-peaked pulse

[a] *Advanced Ultrafast Laser Research Center, University of Electro-Communications, 1-5-1 Chofugaoka, Chofu, Tokyo 182-8585, Japan. E-mail: kobayashi@ils.uec.ac.jp; Fax: +81-42-443-5825; Tel: +81-42-443-5825*
[b] *JST, CREST, 5 Sanbancho, Chiyoda-ku, Tokyo 102-0075, Japan*
[c] *Department of Electrophysics, National Chiao-Tung University, 1001 Ta Hsueh Rd., Hsinchu 300, Taiwan*
[d] *Institute of Laser Engineering, Osaka University, 2-6 Yamada-oka, Suita, Osaka 565-0971, Japan*
† Current address: Max-Planck-Institut für Quantenoptik, Hans-Kopfermann-Strasse 1, D-85748 Garching, Germany.

profile is obtained without satellite pulses and with a smooth spectrum without the use of an external pulse compressor. These features allow for application of the pulse in ultrafast spectroscopy without undue complications. The pulse is easily compressed down to a sub-10 fs pulse duration.[29,30]

In the present article, an 8.7 fs DUV pulse generated by the abovementioned technique is applied to transient absorption spectroscopy with a sub-10 fs time resolution, generating time-resolved data with electronic and vibrational dynamics with a high signal-to-noise ratio for the first time. The sample investigated was an aqueous solution of thymine. The decay dynamics in the electronically excited state and the vibrational dynamics are simultaneously investigated. Sub-picosecond and picosecond decays related to the electronic excited state and a vibrationally hot ground state, respectively, are observed in the thymine measurements. Vibrational modes ranging from low to high frequencies up to 2000 cm^{-1} can be simultaneously probed with the short pulse. From the phase information of the vibrational modes, obtained by Fourier analysis of the oscillatory signal in a difference absorbance trace, it was found that wave packets corresponding to several vibrational modes in both the electronic excited states and ground state are simultaneously induced.

2. Experimental

2.1 Sample preparation

Thymine powder (5-methyluracil) was purchased from Sigma Aldrich and used without further purification. Thymine (65 mg) was dissolved in distilled water (50 ml) to prepare an aqueous solution with a molar concentration of 10 mM and with an absorbance of 1.5 at 4.7 eV for an optical path length of 0.2 mm. The aqueous solution was continuously circulated around a home-made flow cell using a peristaltic pump. The cell had 0.2 mm thick CaF_2 input/output windows and an optical path length of 0.2 mm.

2.2 Sub-10 fs DUV pump–probe spectroscopy setup

The technique of broadband chirped-pulse FWM used for generating a sub-10 fs DUV pulse has been described elsewhere.[29,30] Briefly, a near infrared (NIR) pulse from a Ti:sapphire chirped pulse amplifier was transmitted through glass blocks (10 mm fused silica and 5 mm BK7) and positively chirped. The pulse was then focused into a krypton-gas-filled hollow fiber for spectral broadening by self-phase modulation. A near UV (NUV) pulse generated by frequency doubling of a NIR pulse was negatively chirped with a double-pass prism pair. The broadband NIR pulse and NUV pulse were spatially and temporally synthesized in another hollow core fiber filled with argon gas. By the FWM process in the hollow core fiber, a broadband and negatively chirped DUV pulse was generated. After collimation of the DUV pulse with a concave mirror, the NIR and NUV pulses transmitted through the hollow core fiber and co-propagated with the DUV pulse were carefully eliminated using harmonic separators. For this process, the following setup was used: two low-dispersion dielectric mirrors for s-polarized pulse in the wavelength range of 250–290 nm (Layertec GmbH), two low-dispersion harmonic separators reflecting the DUV wavelength component while transmitting

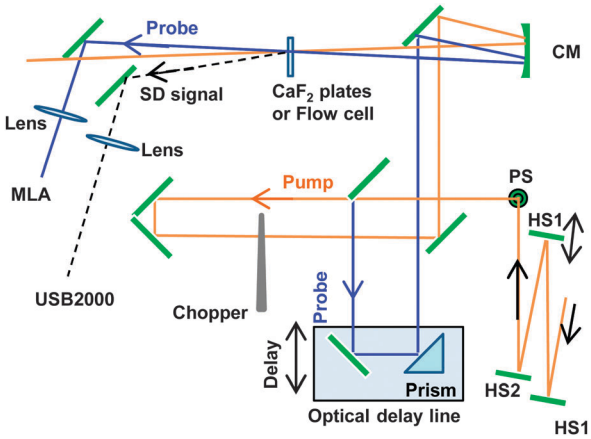

Fig. 1 Experimental setup. HS1, HS2: harmonic separators; PS: periscope; CM: aluminium-coated concave mirror, f = 150 mm; MLA: optical fiber followed by a multi-channel spectrometer and a 128-channel lock-in amplifier.

the NIR wavelength component (Layertec GmbH, HS1 in Fig. 1), and a low-dispersion harmonic separator reflecting the DUV component and transmitting the broadband NUV component (custom product, Layertec GmbH, HS2 in Fig. 1). The pulsed beam was incident to all the harmonic separators with nearly normal incidence. After these separators, the pulse energy of the residual NUV and NIR pulses co-propagating with the DUV pulse (150 nJ) was less than 1 nJ, or less than 1% of the energy of the DUV pulse. The polarization of the horizontally polarized DUV pulse was changed to vertical polarization with a periscope consisting of aluminium mirrors. The pulse was spatially split into two beams[31] using the edge of an aluminium mirror, as shown in Fig. 1. One of the two beams was sent to an optical delay line composed of a stepping motor stage (FS-1020PX, Sigma-Tech), an aluminium mirror, and a fused-silica prism. Due to Fresnel transmission loss from the prism surface, the pulse energy was reduced by a factor of about ten before being used as a probe pulse. The other beam was reflected with a retro reflector with aluminium coating and used as a pump pulse. The pump and probe pulses were focused noncollinearly into a 0.2 mm thick CaF_2 plate. By detecting the self-diffraction (SD) signal generated in the plate with a multi-channel spectrometer (USB2000, Ocean Optics) while scanning the optical delay line, a SD-frequency-resolved-optical gating (SD-FROG) trace was measured for characterization of the pulse shape.[31,32] Another piece of 0.2 mm CaF_2 plate was placed in front of the CaF_2 plate for the SD-signal generation. This was done to pre-compensate for pulse broadening in the input window of the flow cell used in the pump–probe experiments. By optimizing the distance between the harmonic separators in air *via* path length tuning, the pulse duration of the DUV pulse was compressed to the shortest pulse duration possible.[29]

After characterization of the pulse duration, the two CaF_2 plates were replaced with the home-made flow cell. The transmitted probe pulse from the flow cell was focused into a multi-mode fiber which was connected to a multi-channel spectrometer coupled to a 128-channel multi-channel lock-in amplifier.[18] The intensity of the pump pulse was modulated

with a frequency of 500 Hz by an optical chopper for the lock-in detection. The difference absorption spectra were measured over a range of pump–probe delay times from −200 fs to 1800 fs with a step size of 0.2 fs. The pulse energies of the input pump and probe pulses were 40 nJ and 5 nJ, respectively. After repeating the measurement of the thymine sample three times, the sample inside the cell was removed and replaced with pure water and the same measurement procedure repeated. It was found that the blank experiment with water gave no signal other than a coherent artefact at a delay time of around 0 fs as will be discussed later. All the experiments were performed at room temperature (293 K).

3. Results and discussion

3.1 The DUV laser pulse and stationary absorption

The spectrum of the DUV laser pulse measured with a multi-channel spectrometer (USB2000) and that retrieved from the SD-FROG trace are shown in Fig. 2(a). The retrieved spectrum agrees well with that directly measured with the spectrometer, indicating that measurements of the SD-FROG trace and phase retrieval from the trace are accurate enough for evaluation of the pulse temporal profile. The retrieval was performed with commercial software (FROG 3.0, Femtosoft Technologies) and

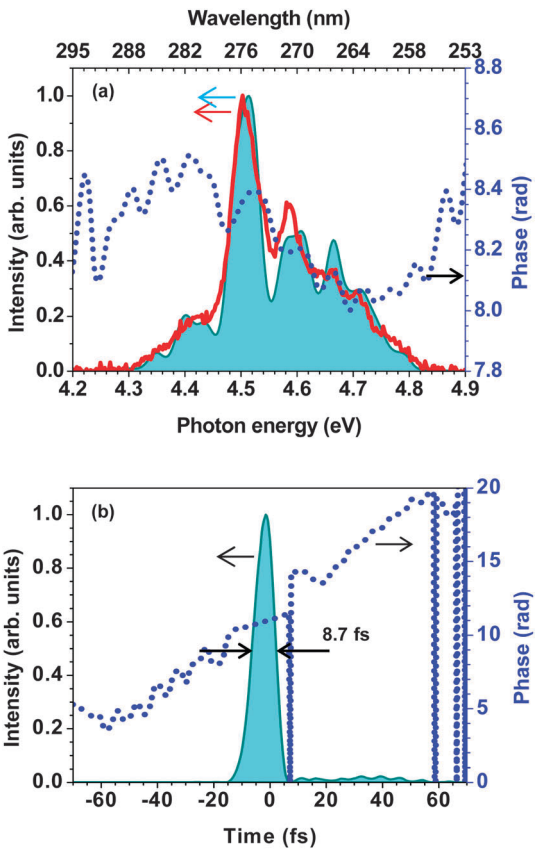

Fig. 2 (a) Spectrum of the DUV pulse measured with a USB2000 multi-channel spectrometer placed in front of the pump–probe setup (solid line) and that retrieved from the SD-FROG measurement (solid area). The spectral phase retrieved from the SD-FROG trace is shown by the dotted line. (b) The temporal intensity profile of the DUV pulse (solid area) and phase (dotted line) from the SD-FROG measurement.

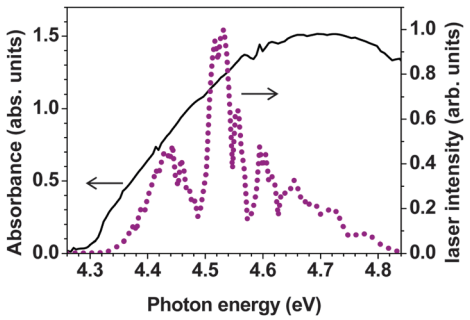

Fig. 3 The stationary absorption spectrum of an aqueous thymine solution measured with a sub-10 fs probe pulse in the pump–probe setup using a 128-channel lock-in detector (solid line). The DUV laser spectrum is also shown (dotted line).

the retrieval error was 0.005. The temporal profile of the intensity of the pulse retrieved from the FROG trace is shown in Fig. 2(b). The profile is free from any satellite pulses and the energy contained in the pedestal component(s) is less than 5% of the main pulse.[29] Thus the pulse is well suited to pump–probe spectroscopy and does not suffer from multiple excitations or multiple probing. The full-width at half-maximum (or pulse duration) of the intensity profile is 8.7 fs. A single pulse shape of sub-10 fs pulse duration can be readily obtained by optimizing the propagation distance of the DUV pulse in air using the chirped-pulse FWM technique.[29,30]

Fig. 3 shows stationary absorption spectra of the aqueous solution of thymine measured with the pump–probe setup. In the same figure, the spectrum of the DUV laser pulse measured with the lock-in amplifier is also depicted. The absorption spectrum has a peak at 4.68 eV, while that of the DUV laser pulse has a peak at 4.52 eV. The spectrum of the DUV pulse overlaps well with the absorption spectrum in the photon energy range below 4.82 eV.

3.2 Dynamics of the electronic excited states

Fig. 4 shows 2D difference absorption spectra of the aqueous thymine solution (average of three measurements (Fig. 4(a)) and pure water (Fig. 4(b)). In the positive delay time range, the thymine spectra exhibit positive ΔA signals at photon energies below 4.42 eV but negative ΔA signals at higher photon energies. The pure water sample does not show any appreciable positive or negative ΔA signals except at delay times of around 0 fs. These signals are also seen at delay times of around 0 fs for the thymine sample, which can be seen more clearly in a difference absorbance trace obtained after averaging in the range between 4.70 eV and 4.75 eV [see Fig. 5]. Specifically, there are intense oscillatory structures in the delay time range between −100 fs and 100 fs, with similar structures apparent for both samples in this delay range. Therefore, the intense oscillatory structure is not attributed to thymine but is considered to be mainly due to a coherent artefact, possibly from two-photon absorption of the DUV pulse by the solvent (water) and/or the CaF_2 windows. The small differences in the strength of the artefact in the range of 4.6–4.8 eV are explained as follows. It is well known that the coherent artefact appears in the same direction as the incoherent signals.[33] Therefore, the negative artefact in the thymine sample occurs due to the negative incoherent signal.

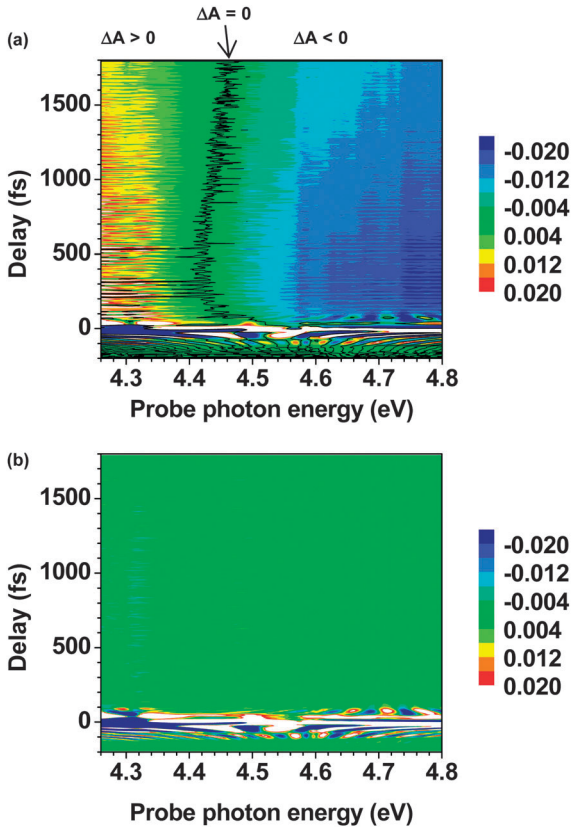

Fig. 4 The measured 2D difference absorption (ΔA) spectra of the (a) aqueous thymine solution and (b) pure water samples.

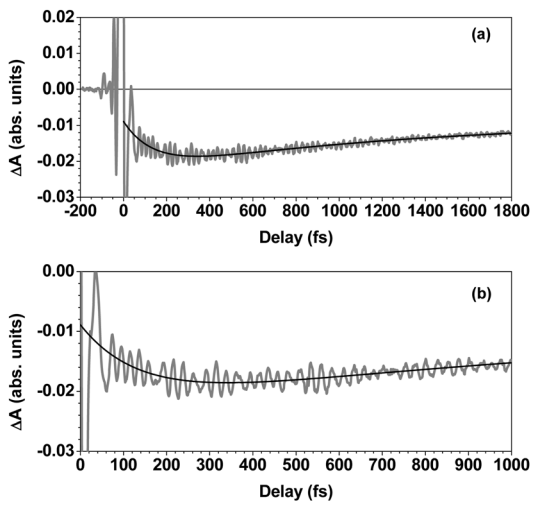

Fig. 5 (a) The measured difference absorbance trace of the thymine sample averaged over the photon energy range between 4.70 and 4.75 eV (gray line). The solid black line indicates the global fitting curve fitted to the experimental data. (b) An expanded view of (a), in which the oscillatory structure present in the difference absorption trace is clearly seen.

Then the difference absorbance of the thymine sample observed to have a negative sign is expected to be affected by the coherent artefact signal. Meanwhile, the artefact signal in water leads to a positive difference absorbance (artificial) signal, and that obtained for thymine at the same photon energy is negative. This negative signal is obtained as a result of the sum of the positive artefact signal and a negative artificial signal arising from thymine related to non-artificial bleaching and/or stimulated emission at a positive time delay. Similar behaviour is observed over nearly all probe photon energies as can be clearly seen if we compare the 2D difference absorption spectra of the thymine sample and water shown in Fig. 4.

To extract the lifetime information from the 2D difference absorption spectrum $\Delta A(\omega, t)$, the trace was fitted by a global fitting procedure using the following fitting function, which allows for three separate species, $\Delta A_1(\omega)$, $\Delta A_2(\omega)$, and $\Delta A_3(\omega)$, and two corresponding time constants, τ_1 and τ_2 (where $\tau_1 < \tau_2$):

$$\Delta A(\omega, t) = \Delta A_1(\omega)\exp(-t/\tau_1) + \Delta A_2(\omega)\exp(-t/\tau_2) + \Delta A_3(\omega), \quad (1)$$

where the third term corresponds to a decay component with a time constant much longer than the experimental delay time (ranging up to 1.8 ps), and ω is the angular frequency of the spectral component of the probe pulse. Fitting was performed in the photon energy range between 4.33 eV and 4.81 eV, for which the relative intensity of the laser is higher than 1% of the peak of the laser spectrum. In this equation, assignment of the exponential coefficients differs depending on whether the sequential model or parallel model is used as discussed later.

Because of the intense coherent artefact in the time range near 0 fs, direct fitting of the trace to the function was difficult and the following step-by-step fitting procedure was carried out to minimize the effect of the artefact. First, the difference absorbance at a delay time longer than 900 fs was fitted to a function consisting of only the second and third terms of eqn (1). At this delay time, the contributions of the first term in eqn (1) and the influence of the coherent artefact on ΔA are negligibly small, allowing fitting to be readily performed without considering the artefact. Indeed, the time constant τ_2 extracted by this fitting did not change substantially when the minimum delay time for fitting was changed in the range from 900 fs to 1300 fs. The time constant τ_2 is thus considered to be correctly estimated by this procedure. The average and standard deviations of τ_2 from six different fittings were τ_2 = 1220 fs and 50 fs, respectively. This estimated time constant τ_2 was then substituted into eqn (1) and the resultant equation was fitted to the 2D difference absorption spectrum to estimate the shorter time constant τ_1. When the minimum probe delay for this fitting was varied from 50 fs to 90 fs, the time constant τ_1 extracted by global fitting of the difference absorbance did not change appreciably, and the average time constant and standard deviation were τ_1 = 140 fs and 7 fs, respectively. For minimum probe delays shorter than 40 fs, the smaller the delay the smaller the time constant, indicating a non-negligible contribution from the coherent artefact as a source of error in determination of the time constant. In Fig. 5, the resulting fitted curve with the estimated time constants of τ_1 = 140 fs and τ_2 = 1220 fs is shown together with the observed difference absorbance trace. Whereas the curves are consistent for delay times longer than 100 fs, there is some discrepancy for delay times below this value due to the coherent artefact, the contribution of which is highly dependent on the probe photon energy as indicated by the observed relation

between the interference structure over time and the inverse of the time separation between the peaks of the pump photon energy and corresponding probe photon energy. However, we believe this effect is minimized by the careful step-by-step procedure outlined above for determination of the parameters.

3.3 Assignment of the species in the relaxation process

To date sub-picosecond electronic decays have been experimentally investigated by two spectroscopic methods: femtosecond pump/probe spectroscopy and fluorescence up-conversion spectroscopy. In the pioneering work of Kohler's group, pump/probe experiments were performed with an experimental instrument response function time of 200 fs using a 150 fs pulse at 267 nm as a pump[10,34] and probe pulses at a limited number of wavelengths.[10] They observed two decay components with lifetimes of 2.8 and 30 ps at 250 nm, a 0.72 ps component at 340 nm, and long-lived components at both wavelengths. The short-lifetime component of 2.8 ps at 250 nm was attributed to a vibrational cooling process and the 30 ps component to an nπ* state. The short-lifetime component of 0.72 ps at 340 nm was attributed to absorption from the lowest ππ* state. However, because of the limited time resolution and number of probe photon energies at which the time-resolved measurement has been done, assignment is a little ambiguous.

The fluorescence upconversion method has been demonstrated by Gustavsson and coworkers.[11] By time-resolved fluorescence spectroscopy with an instrument response function time of about 300 fs, time-resolved ultrafast decay behaviour could be observed with the fluorescence decay dynamics exhibiting components with lifetimes of 195 fs and 633 fs.[11] The short and long decay constants were assigned as relaxations from the L_a state to the L_b state, and the L_b state to the ground state, respectively. However, the dynamics were considerably complicated as admitted by the authors. Such difficulties can readily be appreciated for analysis of a decay signal involving four states fitted by global fitting with a limited signal-to-noise ratio and time resolution, and with additional limitations arising from the fact that the fluorescence is almost always only emitted from the lowest excited state. In the case of thymine particularly, the lowest excited state has the forbidden character of $^1(n\pi^*)$, and it is difficult to analyse the observed data in this case with a four-state model.

Another research methodology used is the theoretical approach. Using various methods, including TD-DFT[11] and the surface-hopping approach,[35] it has generally been agreed that the primary process in thymine after an ultrashort pulse excitation is mainly internal conversion from the strongly allowed ππ* (L_b) state to the forbidden (dark) state of nπ* character. The surface-hopping approach predicts that the lifetimes of the $^1(\pi\pi^*)$ and $^1(n\pi^*)$ states are 17 fs and 420 fs, respectively.[35]

From the studies mentioned above we can start to consider the assignment of the excited species with lifetimes of τ_1 = 140 fs and τ_2 = 1220 fs. These assignments are based on the time-resolved vibrational information obtained from real-time vibrational spectroscopy performed for the first time in the present study. Details on the vibrational information will be discussed later for simplicity.

From the well-accepted theoretical model, the Franck–Condon state of the strongly allowed $^1(\pi\pi^*)$ state is considered to be very close to the conical intersection (CI) and relaxes through the CI to the $^1(n\pi^*)$ state. In this scheme, the first intermediate that appears as an induced absorption ($\Delta A > 0$) in the probe photon energy range of 4.25–4.4 eV is most reasonably assigned to the transition from the $^1(\pi\pi^*)$ state (L_b state) to a higher excited state. The next species that appears may be assigned as the $^1(n\pi^*)$ state, the L_a state, or a charge-transfer (CT) state as discussed by Gustavsson.[12] Among them the L_a state can be ruled out since the transition probability between two L_a states in the L_a family is considered to be smaller than those in the L_b family and this goes against the experimental observation of a readily observed visible time-resolved signal. Also the transition probability between the CT states is expected to be small because the CT character is borrowed from the $^1(\pi\pi^*)$ state by configuration mixing. On the other hand even though the $^1(n\pi^*)$ state is a dark state, to which transition is forbidden from the ground state, there is a possibility of intense transition from the state to the higher $^1(n\pi^*)$ state (here we call it $^1(n\pi^{**})$ state or the $^1(n\pi^{2*})$ state because the transition probability for these transitions can be as high as the corresponding transitions from the $^1(\pi\pi^*)$ state to the $^1(\pi\pi^{**})$ state (or $^1(\pi\pi^{2*})$ state)).

To assign the two species with lifetimes of 140 fs and 1220 fs, we must consider previous experimental and theoretical studies. First there is no doubt that the excited state is the $^1(\pi\pi^*)$ state. The state obtained after relaxation is considered to be the $^1(n\pi^*)$ state based on the following reasons.

Relaxation to another ππ* (L_a) state can be ruled out. It is because if the relaxation were to the L_a state, the fluorescence quantum yield would be higher than the reported value[36] of 10^{-4} as in many of the aromatic molecules. Let us consider the possibility of relaxation to the (nπ*) state. The relaxation times for the $^1(\pi\pi^*)$ and $^1(n\pi^*)$ states in thymine were reported to be 0.72 ps and 30 ps, respectively, from the data obtained by a pump/probe experiment using a 200 fs experimental response function.[10] The same states were estimated to be 195 fs and 633 fs,[11] respectively, for time-resolved fluorescence measurements. Theoretical calculations have predicted lifetimes of 17 fs and 420 fs,[35] respectively, which are consistent with time-resolved photoelectron spectroscopy (TRPE) experiments of thymine in a vacuum ($<$50 fs and 490 fs for shorter and longer time constants, respectively).[37] Since the TRPE experiments were performed in a vacuum it is reasonable to assume that the shorter time constant corresponds to an isolated molecule that does not interact with the thermal bath. Thermal interactions might change the electronic energy levels of the $^1(\pi\pi^*)$ and $^1(n\pi^*)$ states in different ways, possibly resulting in a change in the distance between the Franck–Condon point and the CI point, which is sensitive to the relaxation rate. In addition, the solvent molecules (water) surrounding the thymine molecules also affect the stabilities of the states *via* hydrogen bonding and modify the lifetimes. Considering these factors, our experimental data for both the short- (140 fs) and long-lifetime (1220 fs) components from broadband detection agree moderately well with the fluorescence measurements (195 fs and 633 fs). The observed values for the short-lifetime component of 140 fs in our study and 195 fs by fluorescence measurement may be consistent with the 0.72 ps measured in the previous pump/probe experiment using a relatively long pulse with a 200 fs response time,[10]

which may result in an effectively longer time. The origin of the lifetime of 1220 fs measured in our experiment may also be as follows.

In the 2D difference absorption spectrum, the photon energy at which ΔA is zero, because of cancellation of the positive and negative contributions, decreases with increasing time delay from 0 to 300 fs. When the time delay becomes longer than 300 fs, the difference favors the higher photon energy and increases with increasing time delay. This result may indicate the presence of a vibrational cooling process.[38] A vibrationally excited state in the electronic ground state may be populated *via* a decay process from the excited state $^1(\pi\pi^*)$ with a time constant of 140 fs. Subsequent vibrational cooling may be induced, in which the vibrational energy in the solute is transferred to the solvent.[38] The second time constant of 1220 fs measured in our work is close to the expected time constant for the vibrational cooling.[7,8] However, in fact we attribute this process to relaxation from the $^1(\pi\pi^*)$ state to $^1(n\pi^*)$ state as discussed later. This is based on the vibrational frequency change in this time range as described in the spectrogram analysis section.

The difference absorbance in Fig. 5 does not decay away completely at a probe delay time of 1.8 ps, indicating there is another slower decay component in addition to those with time constants of τ_1 and τ_2. This decay process might correspond to the component with a time constant of 30 ps observed in previous research.[10] In that research, the slow component was assigned as decay to the ground state of a $^1(n\pi^*)$ state formed following decay of the $^1(\pi\pi^*)$ excited state.[10] However, as outlined above this component can be better attributed to thermalization.

Thus the 1220 fs component is attributed either to relaxation from the $^1(n\pi^*)$ state to the ground state or to thermalization. We refer these assignments as Model A and Model B, respectively, hereinafter.

Other factors should also be mentioned here, including the possibility of sequential, parallel, and hybrid processes. In the above discussion, the relaxation path was discussed in terms of a sequential process. However, in real systems the relaxation can be considered to be composed of both sequential and parallel processes, which occur at the same time (hybrid process) because the difference absorbance intensity due to the $^1(n\pi^*)$ state is very small as discussed by Kohler and others.[10] Therefore the relaxation process is most probably described by two simultaneous processes as follows (schematically depicted in Fig. 6),

$$^1(\pi\pi^*) \xrightarrow{k_1} {}^1(n\pi^*) \xrightarrow{k_2} \mathrm{G} \qquad (2)$$

$$^1(\pi\pi^*) \xrightarrow{k_3} \mathrm{G} \qquad (3)$$

where, k_1, k_2, and k_3 indicate the rate constants of the corresponding transitions from $^1(\pi\pi^*)$ to $^1(n\pi^*)$, from $^1(n\pi^*)$ to the ground state, and from $^1(\pi\pi^*)$ to the ground state, respectively.

Based on the results of the pump/probe experiments, it is considered that process (3) has a much greater contribution than process (2).

The meanings of the coefficients $\Delta A_1(\omega)$, $\Delta A_2(\omega)$, and $\Delta A_3(\omega)$ of the corresponding exponential functions are considered to be $\Delta A_1(\omega) = A_1(\omega) - A_2(\omega)$, $\Delta A_2(\omega) = A_2(\omega) - A_3(\omega)$, and $\Delta A_3(\omega) = A_3(\omega)$. The coefficients include the effect due to bleaching of the ground state. Then $A_i(\omega)$ must be replaced with

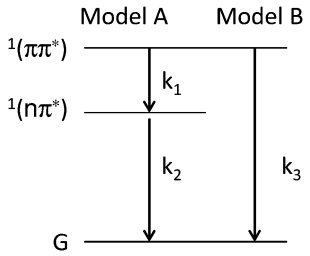

Fig. 6 Schematic energy diagram for Model A, representing relaxation from the $^1(n\pi^*)$ state to the ground state, and Model B, representing thermalization.

$A_i(\omega) - A_0(\omega)$ (i = 1–3) as the relevant parameters. In the case in which both sequential mechanisms occur simultaneously the situation becomes complicated. Regardlessly, the time constant can be fitted in the same way as in the simple case and the parallel processes can in turn be considered based on the relative contributions of each process and their corresponding rates. Despite the complexity of the new parameter definitions, which include both growth and decay processes for the intermediate $^1(n\pi^*)$ state, they can be easily described in terms of an analytical expression using the parallel-sequential model. In this case, $\tau_1 = 1/(k_1 + k_2)$ and $\tau_2 = 1/k_3$. Analysis based on separation of the processes is to be performed in the near future.

3.4 Vibrational dynamics

One of the major features observed in this research is the oscillatory signal in the difference absorbance traces arising from vibrational motion. At a delay time longer than 100 fs, the difference absorbance is found to be modulated at certain frequencies as seen in Fig. 5(b). The period of oscillation is about 20 fs and delay-time dependent. The delay time dependence indicates that several vibrational motions of thymine are impulsively excited and that these act to modulate the difference absorbance. To analyse the vibrational modes contained in the 2D difference absorption spectrum shown in Fig. 4(a), the spectrum was Fourier-transformed along the delay axis to give a 2D Fourier power spectrum showing the distribution of vibrational components existing at each probe photon energy. The resulting Fourier power spectra shown in Fig. 7(a) contain several vibrational components. The same transformation was also done for the pure water sample as shown in Fig. 7(b). At probe photon energies of 4.33 eV and 4.48 eV, numerous vibrational components are observed in the 2D power spectrum of the thymine sample [Fig. 7(a)]. However, these same components are also observed in the power spectrum of the pure water sample, indicating that they do not arise from the vibrational motion of thymine. At 4.33 eV and 4.48 eV, there are valleys in the spectrum of the DUV laser pulse [Fig. 3(a)], and the vibrational components at these photon energies might be due to a small fluctuation in the spectral structure around the valley introducing noise because of the small ΔA. At photon energies of around 4.3 eV, 4.7 eV, and 4.75 eV, on the other hand, there are appreciable vibrational components in the power spectra of the thymine sample that are not present in the power spectra of the pure water sample. These components are hence assigned to the vibrational modes of thymine. For further analysis, the difference absorption spectra [Fig. 4(a)]

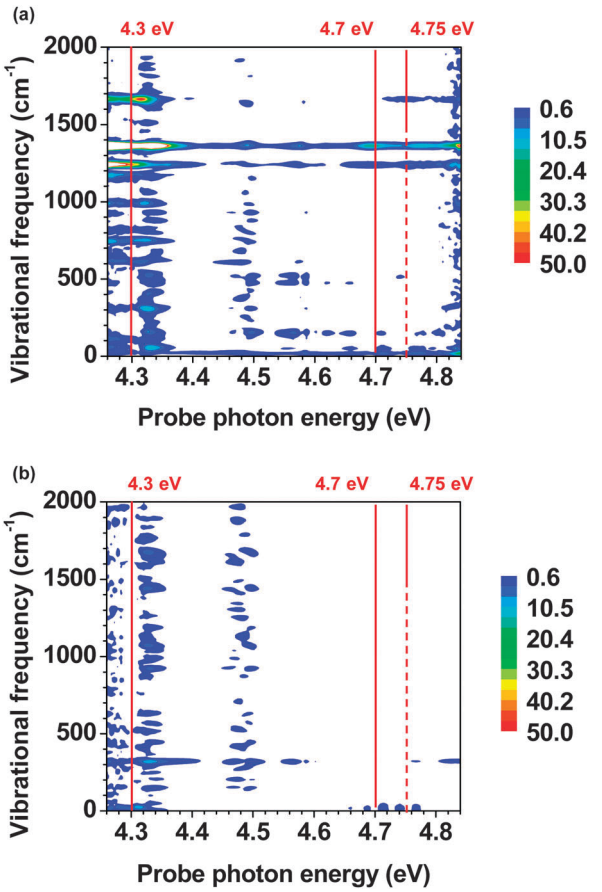

Fig. 7 The 2D Fourier power spectra of the (a) aqueous thymine solution and (b) pure water samples.

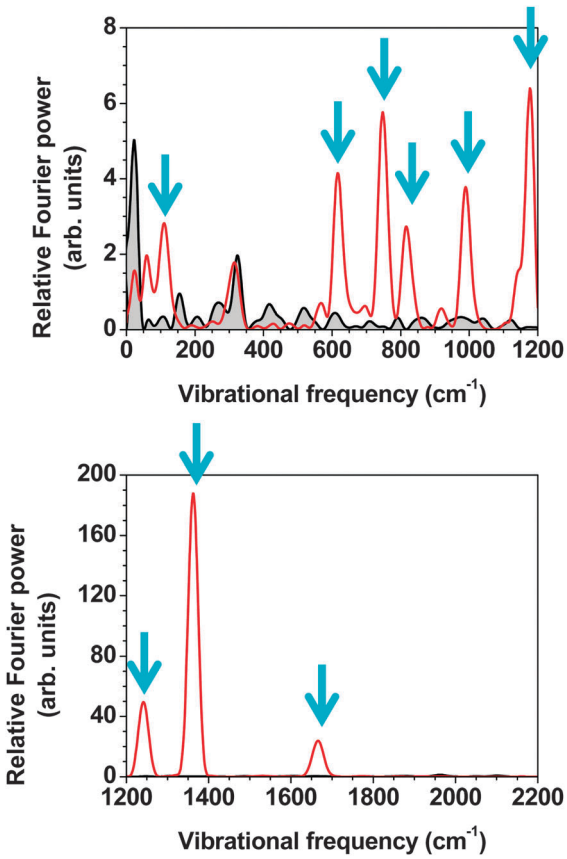

Fig. 8 The Fourier power spectrum of the difference absorbance trace averaged in the photon energy range of 4.28–4.30 eV for the thymine sample (solid line) and the pure water sample (solid area). The arrows indicate the vibrational peaks arising from the thymine molecule.

were averaged over three different photon energy ranges, from 4.28 eV–4.30 eV, 4.69 eV–4.71 eV, and 4.74 eV–4.76 eV. The averaged difference absorbance traces were then Fourier transformed along the delay axis to give the corresponding Fourier power spectra with reduced noise. The power spectrum for the difference absorbance trace averaged at photon energies between 4.28 eV and 4.30 eV is shown in Fig. 8. There are three intense peaks in the frequency range above 1200 cm^{-1} and six peaks with relatively low intensities in the lower frequency range. The intensities of these peaks are much higher than the intensities of the corresponding frequency components in the Fourier spectrum of water, and hence arise from the molecular vibration of thymine. The vibrational frequencies of the three strong peaks are 1241, 1362, and 1666 cm^{-1} and those of the weak peaks are 110, 616, 748, 816, 989, and 1177 cm^{-1}, as determined by the first derivative of the Fourier power spectrum. In the power spectrum of the difference absorbance trace averaged between 4.69 and 4.71 eV, for which the absorbance change is negative (Fig. 4(a)), vibrational peaks were observed at 1170, 1240, and 1362 cm^{-1}. The wave packet inducing modulation in the electronic transition can be attributed to an excited state because the initial state of the probing electronic transition under modulation is not the ground state but the excited state being populated. However, another assignment is also possible as discussed in the following.

The time-resolved spectral signal extends into the range of the probe spectrum from 4.32 to 4.82 eV and heavily overlaps with the ground state absorption of thymine. In this case, even in the negative absorbance range of 4.45 eV, there is the possibility of contribution to ground-state bleaching and even stimulated emission. Even though the fluorescence quantum efficiency is very low, time resolved measurements can resolve extremely weak spontaneous emission transitions without any difficulty *via* stimulated emission when the pulse duration is shorter than the lifetime of this very weak fluorescent system due to efficient nonradiative transition.

For the power spectrum of the trace averaged between 4.74 and 4.76 eV, for which the absorbance change is negative (Fig. 4(a)), a vibrational peak at 1665 cm^{-1} was observed, which was maximum around this probe photon energy. The wave packet inducing the modulation in pump–probe traces can be considered to belong to the ground state, although assignment to an excited state is also possible, because the initial and final states are the excited state and the ground state, respectively. This expectation of the ground-state process is supported later by the calculated initial phase of the vibration. The vibrational frequencies obtained are summarized in Table 1.

The Raman spectrum of thymine has been investigated by several researchers.[39–41] The vibrational frequencies reported depend on the type of sample measured. When comparing the vibrational frequencies obtained in previous reports for thymine measured in aqueous solution[41] and in the solid phase,[39] some

Table 1 The peak frequencies and phases of the vibrational modes obtained in the present work and from previous reports. Abbreviations: w, weak; m, medium; s, strong; vs, very strong

Frequency/cm^{-1}			Present research Relative FT amplitude	Phase (π)			Previous research Frequency/cm^{-1}			
4.28–4.30 eV	4.69–4.71 eV	4.74–4.76 eV	4.28–4.30 eV	4.28–4.30 eV	4.69–4.71 eV	4.74–4.76 eV	Ref. 41	Ref. 39	Theory, ref. 40	Assignment
110(w)			0.12	0.53					111	Ring deformation
616(w)			0.15	−0.68			616(w)	617(s)	608	C═O bending
748(w)			0.17	−0.64			752(w)	740(s)	766	C═O wagging
816(w)			0.12	0.95			813(w)	804(m)	805	Ring deformation
989(w)			0.14	−0.71				984(m)	963	C–N stretch + CH_3 rocking
1177(w)	1170		0.18	−0.89	0.39		1168(w)	1156(w)	1196	C–N stretch + C–H bending
1241(s)	1240		0.51	−0.43	0.38		1237(s)	1247(w)	1224	C–CH_3 stretch + ring stretch
1362(vs)	1362		1	−0.35	0.43		1359(vs)	1369(vs)	1371	C–H bend + C═C stretch
1666(s)		1665	0.36	−0.41		0.41	1662(vs)	1671(vs)	1702	C═C stretch

of the modes are nearly the same but others do not match, as shown in Table 1. In the former report, an aqueous solution of thymine and a pump pulse at 266 nm were utilized, which is similar to the present research except the pulse width. The peak frequencies of the vibrational modes observed in the present research are in good agreement with those reported in studies on resonance Raman scattering,[41] and are within 4 cm^{-1} (Table 1) with the exception of the mode at 1177 cm^{-1}. By considering the assignments of previous experimental reports[41] and those obtained using density functional theory (DFT) calculations,[40] we can assign the vibrational frequency components observed in our research as shown in Table 1. These assignments include various modes such as ring deformation, C═O bending, C–N stretching, and C═C stretching. The most intense three vibrational modes, at 1240, 1362, and 1666 cm^{-1}, were assigned to a C–CH_3 stretch + a ring stretch, a C–H bend + a C═C stretch, and a C═C stretch, respectively.[40,41] Additionally, the mode at 1666 cm^{-1} might have some contribution from a C═O stretch.

Let us now discuss the phases of the vibrational modes obtained by the Fourier analysis. In principle, when the vibrational phase is ±π/2, the vibrational motion is assigned to the mode in the electronic ground state, while when the phase is 0 or π, it is assigned to the electronically excited state. As listed in Table 1, the phases of almost all the vibrational modes are at around ±π/2, suggesting that they arise from the electronic ground state. On the other hand, the phases of the modes at 816 and 1177 cm^{-1} (at 4.29 eV) are at around π and may be assigned to the modes in the electronic excited state. Concerning the mode at 1177 cm^{-1}, a vibrational mode with nearly the same frequency is observed in the high photon energy range (4.69–4.71 eV). The frequency of this mode is 1170 cm^{-1} and the phase is close to π/2, indicating a ground state assignment. Based on the results of previous research, the modes at 1177 cm^{-1} and 1170 cm^{-1} may be assigned to a C–N stretch and a C–H bending mode.[40,41]

The mode at 1177 cm^{-1} is a little higher than that at 1170 cm^{-1} observed for the negative ΔA range. The latter frequency is considered to be due to the ground state and close to that of Raman at 1168 cm^{-1} due to the ground state.[40,41] This feature is considered to be due to ππ* excitation, in which the π electrons are more uniformly distributed over the C═C bonds and C–N bonds forming the pyrimidine ring of thymine.

3.5 Spectrogram analysis

To investigate the vibrational dynamics in more detail in terms of the modes at 1177 and 1170 cm^{-1}, averaged difference absorbance traces obtained in the range 4.28–4.30 eV and 4.69–4.71 eV, respectively, were analysed by spectrogram analysis.[21,42,43] The time window used here was a Blackman function with a width of 1500 fs, which is selected based on a compromise between the time resolution and the frequency resolutions. The vibrational component at 1240 cm^{-1} is much stronger than the component at 1177 cm^{-1}, and the frequency difference between 1240 and 1177 cm^{-1} is small. Hence, the window was selected to be the longest duration possible but not too long that information on the instantaneous frequency change with respect to time would be lost. Subsidiary calculation was made so that the resolution is not lost even with the relatively broad width mentioned above using some model calculation (data not shown).

Because an artificial oscillatory signal exists at a delay time at around 0 fs, the spectrogram analysis was performed only for delay times longer than 60 fs. The results of the spectrogram analysis are shown in Fig. 9, in which the spectrograms for thymine solution and pure water samples are shown. Up to a delay time of 400 fs, a signal appears in the spectrogram due to the coherent artefact in the vibrational real-time trace, which can also be seen in the spectrogram for the water sample [Fig. 9(b)]. The artificial signal may be due to the oscillatory structure originating from the coherent artefact in the difference absorption spectrum, which is small but still exists in the delay time range of 60–100 fs. In the delay range longer than 400 fs, the amplitude of the artificial signal is small as shown in both Fig. 9(b) and (d). The spectrograms for the thymine sample in the same delay time range, Fig. 9(a) and (b), seem to be not appreciably distorted by the effect of the artificial signal. In the spectrogram shown in Fig. 9(a), there is a strong vibrational component at around 1240 cm^{-1}. At time delays longer than 500 fs, a sideband is generated near the 1240 cm^{-1} component and the frequency of the band continuously red-shifts (to lower frequencies)

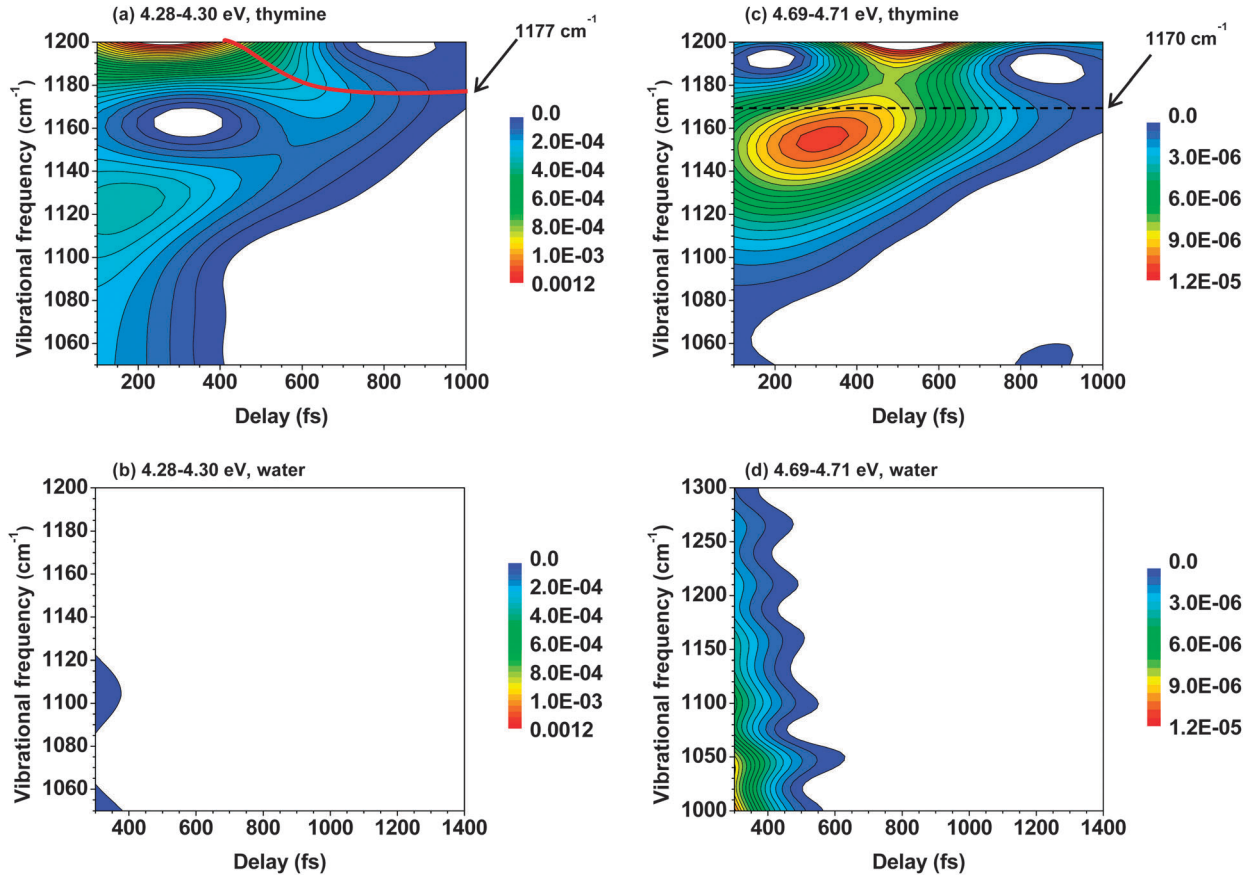

Fig. 9 Spectrogram for the difference absorbance spectra averaged between 4.28 and 4.30 eV for the (a) thymine and (b) pure water sample, and that averaged between 4.69 and 4.71 eV for the (c) thymine and (d) pure water sample.

until it reaches 1177 cm^{-1} with a time delay of about 200–300 fs. It is difficult to precisely determine the time constant because of convolution with the gate function. However, it can be shown that using the gated window methods for determining the instantaneous frequency, as used here in the spectrogram analysis, the time resolution is much less affected as mentioned above than the case of population. The observed red shift is missing in the spectrogram obtained for the photon energy range from 4.69 to 4.71 eV [Fig. 9(c)].

In the following, we consider mainly Model A as discussed above, but if we instead attribute the long-lifetime component to thermalization, as given in Model B, similar conclusions can be made.

The above results indicate that the mode at 1177 cm^{-1} is generated after the decay of the $^1(\pi\pi^*)$ state whereas the mode at 1170 cm^{-1} is not. This is consistent with the observed phases of the vibrational modes at 1177 cm^{-1} and 1170 cm^{-1}, and their consequent assignment to the electronic excited state and ground state, respectively.

There is another possible explanation for the red shift. If the signal in the time range between 500 fs and 1000 fs were due to the $^1(n\pi^*)$ state, then the frequency reduction taking place before recovery of the ground-state may be due to the process from the $^1(\pi\pi^*)$ state to the $^1(n\pi^*)$ state. Here, despite the contribution being small, we are able to claim that we could detect the difference between the excited and non-excited conditions by a lock-in detection method. The red shift may be due to a reduction in the bond order for the transition process from the $^1(\pi\pi^*)$ state to the $^1(n\pi^*)$ state. The amount of electrons flowing from the π orbital to the π^* orbital during this transition process is expected to be greater than that from the non-bonding orbital to the π^* orbital. Therefore the bond-order uniformities in $n\pi^*$ excitation is not as strong as those in $\pi\pi^*$ excitation.

In order to validate the above discussion, a similar analysis was done for the mode at 1666 cm^{-1}, assigned to C=C stretching and C=O stretching, which would be most affected by a change in bond order upon excitation. The calculated results showed an increase in the frequency over a similar time scale (data not shown), which is consistent with our expectation, *i.e.* an increase in the C=C bond order concomitant with a decrease in the C–N bond order in the pyrimidine ring as a result of relaxation from the photo-excited $^1(\pi\pi^*)$ state to the $^1(n\pi^*)$ state or to the ground state. However, in this case the effect of interference with more intense modes adversely affects the data and the above mechanism of the C=C stretching cannot be reliably confirmed. One method which we plan to use to improve the signal-to-noise ratio and the subsequent analysis is the "optical kernel method".[44] In this way, by simultaneously observing the electronic relaxation and molecular vibrational dynamics, we can identify the species observed by simple decay of the electronic transition probability.

Also spectral information could be obtained for as many as 128 wavelengths, which would aid assignment in case quantum chemical calculations can provide a more detailed understanding of excited states in the future.

4. Conclusions

In summary, sub-10 fs single DUV laser pulses have been applied to ultrafast spectroscopy in the DUV wavelength range for the first time. The short DUV pulses are generated by a chirped-pulse FWM technique. The electronic excited state decay dynamics and vibrational dynamics of an aqueous solution of thymine were simultaneously probed with a time resolution of a few femtoseconds. Two time constants were extracted from the difference absorption spectra measured in the time range up to 1800 fs. A time constant of 140 fs can be assigned to the lifetime of the $^1(\pi\pi^*)$ state. A time constant of 1220 fs can be assigned to relaxation of the $^1(n\pi^*)$ state. This assignment was made based on the information of vibrational dynamics, including the data of the initial vibrational phase, obtained for the first time in the present work. This time constant may also be assigned to a vibrational cooling process, in which the vibrational energy in the thymine is transferred to the surrounding water molecules.

Oscillatory structures are observed in the difference absorption spectra due to vibrational motions induced in thymine. By Fourier analysis of the difference absorbance traces, vibrational modes up to 1666 cm^{-1} are observed. The most intense three modes, at 1240, 1362, and 1666 cm^{-1}, are assigned to a C–CH_3 stretch + a ring stretch, a C–H bend + a C=C stretch, and a C=C stretch + a C=O stretch, respectively. All these modes correspond to ground-state molecular vibrations. Vibrational modes which may be assigned to the electronic excited state are also observed at 816 cm^{-1} and 1177 cm^{-1}, both of which have vibrational phases at near π. The modes are assigned to a ring deformation and a C–N stretching + a C–H bending, respectively. For the mode at 1177 cm^{-1}, a mode with slightly different frequency is observed at 1170 cm^{-1} in the high photon energy range. This is assigned to a vibrational mode in the electronic ground state based on an observed vibrational phase of near $\pi/2$. The phases of the observed vibrational modes are not exact integer or half-integer multiples of π. This is probably due to a mixed contribution of excited state and ground state modes induced by the wave packets in both the states. The phase deviation may also be due to a small deviation in the frequency from the true value. For example, a possible error in the determination of the frequency of 5 cm^{-1}, which is only 0.3% (corresponding to an error in the time period of only 0.11 fs) deviation from the correct frequency in the case of a 1500 cm^{-1} mode, can induce a deviation of 0.3π in the phase if the amplitude does not decay during the course of probe delay time.

Spectrogram analysis has shown that the mode at 1177 cm^{-1} is generated at a longer time delay than 500 fs and is subsequent to the decay of the first electronic excited state. These results indicate that the mode at 1177 cm^{-1} is generated after the decay of the $^1(\pi\pi^*)$ state whereas the mode at 1170 cm^{-1} is not. This is consistent with the phases of the vibrational modes at 1177 cm^{-1} and 1170 cm^{-1}, and their assignment to the electronic excited state and ground state, respectively. At time delays longer than 500 fs, a sideband is generated near the component at 1240 cm^{-1} and the frequency of the band continuously red-shifts (shifts to lower frequencies), ultimately reaching 1177 cm^{-1}.

Another possible explanation for the red shift was considered. If the signal in the time range between 500 fs and 1000 fs is considered to be due to the $^1(n\pi^*)$ state, then the reduction in frequency taking place before the ground-state recovery may be due to the relaxation process from the $^1(\pi\pi^*)$ state to the $^1(n\pi^*)$ state. Despite the contribution being small, we can detect the difference between the excited and non-excited states by a lock-in detection method.

By these experimental results and analysis, it is demonstrated that sub-10 fs DUV laser pulses can be used effectively in ultrafast spectroscopy. It is expected that the present method and a variety of related methods, including the use of the sub-10 fs DUV pulse as a pump source in time-resolved fluorescence spectroscopy, DUV pump–NUV probe spectroscopy using a sub-10 fs NUV light source obtained with self-phase modulation,[45] DUV pump–Vis probe spectroscopy with application of few-cycle visible pulses from a noncollinear optical parametric amplifier,[46] and DUV-pump–IR-probe spectroscopy, will greatly stimulate research into the ultrafast photochemical dynamics observed under DUV irradiation, especially in regard to biologically significant molecules such as DNA and proteins.

Acknowledgements

The authors would like to thank Dr Jun Liu for valuable discussions on the construction of the DUV laser. This work was supported by the Core Research for Evolutional Science and Technology (CREST) Program of the Japan Science and Technology Agency (JST), the National Science Council of the Republic of China, Taiwan (NSC 98-2112-M-009-001-MY3), and a Grant from the Ministry of Education, Aiming for Top University (MOE ATU) Program, at the National Chiao-Tung University (NCTU). Part of this work was performed as a joint research project with the Institute of Laser Engineering, Osaka University under Contract No. A3-01.

References

1 C. E. Crespo-Hernández, B. Cohen, P. M. Hare and B. Kohler, *Chem. Rev.*, 2004, **104**, 1977–2019.
2 B. Kohler, *J. Phys. Chem. Lett.*, 2010, **1**, 2047–2053.
3 C. E. Crespo-Hernández, B. Cohen and B. Kohler, *Nature*, 2005, **436**, 1141–1144.
4 W. J. Schreier, T. E. Schrader, F. O. Koller, P. Gilch, C. E. Crespo-Hernández, V. N. Swaminathan, T. Carell, W. Zinth and B. Kohler, *Science*, 2007, **315**, 625–629.
5 N. K. Schwalb and F. Temps, *Science*, 2008, **322**, 243–245.
6 T. Gustavsson, R. Improta and D. Markovitsi, *J. Phys. Chem. Lett.*, 2010, **1**, 2025–2030.
7 A. Reuther, A. Laubereau and D. N. Nikogosyan, *J. Phys. Chem.*, 1996, **100**, 5570–5577.
8 A. Reuther, H. Iglev, R. Laenen and A. Laubereau, *Chem. Phys. Lett.*, 2000, **325**, 360–368.
9 W.-M. Kwok, C. Ma and D. L. Phillips, *J. Am. Chem. Soc.*, 2008, **130**, 5131–5139.
10 P. M. Hare, C. E. Crespo-Hernández and B. Kohler, *Proc. Natl. Acad. Sci. U. S. A.*, 2007, **104**, 435–440.
11 T. Gustavsson, Á. Bányász, E. Lazzarotto, D. Markovitsi, G. Scalmani, M. J. Frisch, V. Barone and R. Improta, *J. Am. Chem. Soc.*, 2006, **128**, 607–619.
12 T. Gustavsson, Á. Bányász, R. Improta and D. Markovitsi, *J. Phys.: Conf. Ser.*, 2011, **261**, 012009.
13 A. T. Krummel and M. T. Zanni, *J. Phys. Chem. B*, 2006, **110**, 13991–14000.
14 J. R. Dwyer, L. Szyc, E. T. J. Nibbering and T. Elsaesser, *J. Phys. Chem. B*, 2008, **112**, 11194–11197.

15 M. Towrie, G. W. Doorley, M. W. George, A. W. Parker, S. J. Quinn and J. M. Kelly, *Analyst*, 2009, **134**, 1265–1273.
16 Ł. Szyc, M. Yang, E. T. J. Nibbering and T. Elsaesser, *Angew. Chem., Int. Ed.*, 2010, **49**, 3598–3610.
17 T. Kobayashi, T. Saito and H. Ohtani, *Nature*, 2001, **414**, 531–534.
18 N. Ishii, E. Tokunaga, S. Adachi, T. Kimura, H. Matsuda and T. Kobayashi, *Phys. Rev. A: At., Mol., Opt. Phys.*, 2004, **70**, 023811.
19 D. Polli, G. Cerullo, G. Lanzani, S. De Silvestri, H. Hashimoto and R. J. Cogdell, *Biophys. J.*, 2006, **90**, 2486–2497.
20 L. Lüer, C. Gadermaier, J. Crochet, T. Hertel, D. Brida and G. Lanzani, *Phys. Rev. Lett.*, 2009, **102**, 127401.
21 I. Iwakura, A. Yabushita and T. Kobayashi, *J. Am. Chem. Soc.*, 2009, **131**, 688–696.
22 T. Virgili, L. Lüer, G. Cerullo, G. Lanzani, S. Stagira, D. Coles, A. J. H. M. Meijer and D. G. Lidzey, *Phys. Rev. B: Condens. Matter Mater. Phys.*, 2010, **81**, 125317.
23 C. G. Durfee, S. Backus, H. C. Kapteyn and M. M. Murnane, *Opt. Lett.*, 1999, **24**, 697–699.
24 P. Baum, S. Lochbrunner and E. Riedle, *Appl. Phys. B: Lasers Opt.*, 2004, **79**, 1027–1032.
25 T. Fuji, T. Horio and T. Suzuki, *Opt. Lett.*, 2007, **32**, 2481–2483.
26 S. A. Trushin, K. Kosma, W. Fuss and W. E. Schmid, *Opt. Lett.*, 2007, **32**, 2432–2434.
27 U. Graf, M. Fiess, M. Schultze, R. Kienberger, F. Krausz and E. Goulielmakis, *Opt. Express*, 2008, **16**, 18956–18963.
28 F. Reiter, U. Graf, M. Schultze, W. Schweinberger, H. Schröder, N. Karpowicz, A. M. Azzeer, R. Kienberger, F. Krausz and E. Goulielmakis, *Opt. Lett.*, 2010, **35**, 2248–2250.
29 Y. Kida, J. Liu, T. Teramoto and T. Kobayashi, *Opt. Lett.*, 2010, **35**, 1807–1809.
30 Y. Kida and T. Kobayashi, *J. Opt. Soc. Am. B*, 2011, **28**, 139–148.
31 S. Backus, J. Peatross, Z. Zeek, A. Rundquist, G. Taft, M. M. Murnane and H. C. Kapteyn, *Opt. Lett.*, 1996, **21**, 665–667.
32 D. Kane and R. Trebino, *IEEE J. Quantum Electron.*, 1993, **29**, 571–579.
33 C. C. Hayden and R. Trebino, *Appl. Phys. B: Photophys. Laser Chem.*, 1990, **51**, 350–357.
34 J. M. L. Pecourt, J. Peon and B. Kohler, *J. Am. Chem. Soc.*, 2001, **123**, 10370–10378.
35 Z. Lan, E. Fabiano and W. Thiel, *J. Phys. Chem. B*, 2009, **113**, 3548–3555.
36 M. Daniels and W. Hauswirth, *Science*, 1971, **171**, 675–677.
37 S. Ullrich, T. Schultz, M. Z. Zgierski and A. Stolow, *Phys. Chem. Chem. Phys.*, 2004, **6**, 2796–2801.
38 C. T. Middleton, K. de La Harpe, C. Su, Y. K. Law, C. E. Crespo-Hernández and B. Kohler, *Annu. Rev. Phys. Chem.*, 2009, **60**, 217–239.
39 J. De Gelder, K. De Gussem, P. Vandenabeele and L. Moens, *J. Raman Spectrosc.*, 2007, **38**, 1133–1147.
40 S. Yarasi, B. E. Billinghurst and G. R. Loppnow, *J. Raman Spectrosc.*, 2007, **38**, 1117–1126.
41 S. Yarasi, P. Brost and G. R. Loppnow, *J. Phys. Chem. A*, 2007, **111**, 5130–5135.
42 T. Kobayashi, Y. Wang, Z. Wang and I. Iwakura, *Chem. Phys. Lett.*, 2008, **466**, 50–55.
43 T. Kobayashi, J. Du, W. Feng and K. Yoshino, *Phys. Rev. Lett.*, 2008, **101**, 037402.
44 T. Saito and T. Kobayashi, *J. Phys. Chem. A*, 2002, **106**, 9436–9441.
45 J. Liu, K. Okamura, Y. Kida, T. Teramoto and T. Kobayashi, *Opt. Express*, 2010, **18**, 20645–20650.
46 A. Baltuska, T. Fuji and T. Kobayashi, *Opt. Lett.*, 2002, **27**, 306–308.

